Int J Cardiovasc Imaging (2017) 33:1101–1110
DOI 10.1007/s10554-016-1003-0

ORIGINAL PAPER

Assessment of endothelial shear stress in patients with mild or intermediate coronary stenoses using coronary computed tomography angiography: comparison with invasive coronary angiography

Dexiao Huang[1] · Takashi Muramatsu[2] · Yingguang Li[3] · Wenjie Yang[4] · Yasuomi Nagahara[2] · Miao Chu[5] · Pieter Kitslaar[3] · Masayoshi Sarai[2] · Yukio Ozaki[2] · Yiannis S. Chatzizisis[6] · Fuhua Yan[4] · Johan H. C. Reiber[3] · Renhua Wu[1] · Jun Pu[7] · Shengxian Tu[5]

Received: 25 August 2016 / Accepted: 18 October 2016 / Published online: 31 October 2016

Abstract Characterization of endothelial shear stress (ESS) may allow for prediction of the progression of atherosclerosis. The aim of this investigation was to develop a non-invasive approach for in vivo assessment of ESS by coronary computed tomography angiography (CTA) and to compare it with ESS derived from invasive coronary angiography (ICA). A total of 41 patients with mild or intermediate coronary stenoses who underwent both CTA and ICA were included in the analysis. Two geometrical models of the interrogated vessels were reconstructed separately from CTA and ICA images. Subsequently, computational fluid dynamics were applied to calculate the ESS, from which ESS_{CTA} and ESS_{ICA} were derived, respectively. Comparisons between ESS_{CTA} and ESS_{ICA} were performed on 163 segments of 57 vessels in the CTA and ICA models. ESS_{CTA} and ESS_{ICA} were similar: mean ESS: 4.97 (4.37–5.57) Pascal versus 4.86 (4.27–5.44) Pascal, $p=0.58$; minimal ESS: 0.86 (0.67–1.05) Pascal versus 0.79 (0.63–0.95) Pascal, $p=0.37$; and maximal ESS: 14.50 (12.62–16.38) Pascal versus 13.76 (11.44–16.08) Pascal, $p=0.44$. Good correlations between the ESS_{CTA} and the ESS_{ICA} were observed for the mean ($r=0.75$, $p<0.001$), minimal ($r=0.61$, $p<0.001$), and maximal ($r=0.62$, $p<0.001$) ESS values. In conclusion, geometrical reconstruction by CTA yields similar results to ICA in terms of segment-based ESS calculation in patients with low and intermediate stenoses. Thus, it has the potential of allowing combined local hemodynamic and plaque morphologic information for risk stratification in patients with coronary artery disease.

Keywords Computational fluid dynamics · Endothelial shear stress · Coronary computed tomography angiography · Invasive coronary angiography

Abbreviations

ADCT	320-Row area detector CT
CFD	Computational fluid dynamics
CTA	Computed tomography angiography
DSCT	128-Slice dual-source CT
ESS	Endothelial shear stress
ICA	Invasive coronary angiography
IVUS	Intravascular ultrasound
MLA	Minimum lumen area
OCT	Optical coherence tomography
QCA	Quantitative coronary angiography
VFR	Volumetric flow rate

✉ Renhua Wu
cjr.wurenhua@vip.163.com

✉ Jun Pu
pujun310@hotmail.com

1 Department of Medical Imaging, The Second Affiliated Hospital, Medical College of Shantou University, Shantou 515041, Guangdong, People's Republic of China

2 Department of Cardiology, Fujita Health University Hospital, Toyoake, Japan

3 Division of Image Processing, Department of Radiology, Leiden University Medical Center, Leiden, The Netherlands

4 Department of Radiology, Rui Jin Hospital, Shanghai Jiao Tong University School of Medicine, Shanghai, China

5 Biomedical Instrument Institute, School of Biomedical Engineering, Shanghai Jiao Tong University, Shanghai, China

6 Cardiovascular Biology and Biomechanics Laboratory, Cardiovascular Division, University of Nebraska Medical Center, Omaha, NE, USA

7 Department of Cardiology, Ren Ji Hospital, Shanghai Jiao Tong University School of Medicine, Shanghai, China

Introduction

It is vastly held that regions with low endothelial shear stress (ESS) are prone to the buildup of atherosclerotic plaques, which contributes to the development of coronary artery disease [1–6]. Uneven regional distribution of ESS might explain the uneven distribution of atheroma plaques in specific anatomic coronary settings, such as curved vessels or bifurcations [2, 7–9]. Assessment of local ESS may be useful for risk stratification in patients that may have coronary artery disease. Nevertheless, it is impossible to measure shear stress directly in vivo. By using computational fluid dynamics (CFD), ESS can be calculated if accurate vessel geometry is reconstructed [10]. Many CFD studies have used invasive imaging techniques such as invasive coronary angiography (ICA), intravascular ultrasound (IVUS) and optical coherence tomography (OCT) [7, 11–13] for geometrical reconstruction, which are adequate in a high-risk patient population. For a low-to-intermediate patient population, coronary computed tomography angiography (CTA) has emerged as an important non-invasive tool for imaging all coronary arteries. The entire coronary tree structure can now be reconstructed from CTA images and ESS can be evaluated non-invasively [14–16]. This is particularly important since the conventional single-conduit model that neglects side branches in the 3D reconstruction might lead to inaccurate computation of ESS [13, 17]. Despite the feasibility of ESS computation by CTA being demonstrated in previous studies [14–16], the impact of the lower imaging resolution of CTA on the computation of ESS is unknown. To date, there has been no direct comparison of CTA-derived ESS and ICA-derived ESS when applying coronary tree reconstruction in both computations. The aim of this study was to develop a CTA-based computational method for ESS assessment and to validate it in a low-to-intermediate patient population using coronary tree reconstruction from ICA images. In addition, the impact of two different inlet flow profiles; i.e., pulsatile versus steady, on the computation of ESS was also investigated.

Methods

Study design

This retrospective and observational study enrolled 44 patients with mild or intermediate coronary stenosis who received both coronary CTA and ICA at Fujita Health University Hospital, Toyoake, Aichi, Japan, and at Ruijin Hospital, Shanghai Jiao Tong University School of Medicine, Shanghai, China. Coronary CTA and ICA images were used to separately reconstruct two geometrical models of the interrogated vessels, including the side branches. Subsequently, CFD was used to calculate the ESS, and ESS_{CTA} and ESS_{ICA} were derived. Using the same segments that defined by the consecutive side branches in the CTA and ICA models, comparisons were made between ESS_{CTA} and ESS_{ICA}. The study was approved by the institutional review board.

Study population

The study population in this study was the same employed in a previous study [18]. Simple random sampling method was used to choose the patients who underwent both CTA and ICA for post hoc analysis. The inclusion criteria were the following: (1) CTA was performed <60 days before ICA, (2) age >18 years, (3) major epicardial coronary arteries having mild or intermediate de novo lesions (30–70 % in diameter stenosis by visual estimation), (4) no screened lesion in the ostial left main or ostial right coronary artery, (5) nitroglycerine was given prior to the angiographic acquisitions, and (6) two angiographic projections >25° apart were recorded by flat-panel X-ray systems. The exclusion criteria were: (1) presence of chronic total occlusion, (2) allergy with iodine contrast medium, (3) poor ICA image quality for delineation of lumen contours, (4) excessive overlap or foreshortening (>90 %) in ICA images, and (5) the presence of motion artifacts in the 3D reconstructed CTA images.

Coronary CTA image acquisition and geometrical reconstruction [18]

A 320-slice area detector CT (ADCT) scanner (Aquilion ONE ViSION Edition, Toshiba Medical Systems, Otawara, Japan) or a second-generation dual-source 128-DSCT scanner (SOMATOM Definition Flash, Siemens Medical Solutions, Forchheim, Germany) was used to obtain coronary CTA images according to the clinical protocols in the local hospitals.

320-Detector row and dual-source CT image acquisition [18]

A 320-detector ADCT scanner system with a collimation of 320×0.5 mm, pixel size of 0.35×0.35 mm, and rotation time of 275 or 350 ms was used for patient scanning. Prospective ECG-gating in one heart beat with a HR of <65 beats/min for half reconstruction and in two or three heart beats with a HR of ≥65 beats/min for segment reconstruction were used for axial scans. A total of 245 mg I/kg of contrast medium was continuously injected for 12 s followed by 20 ml saline at 3.0 ml/s for the contrast-enhanced

scan. A slice thickness of 0.5 mm and reconstruction interval of 0.25 mm was used for image reconstruction.

A second-generation 128-slice dual-source CT (DSCT) scanner was used that had a collimation of $2\times128\times0.6$ mm, pixel size of 0.36 ± 0.04 mm (range 0.30–0.48 mm), and gantry rotation time of 280 ms, Patients were studied with one of three image acquisition protocols, which were: (1) prospectively ECG-triggered axial acquisition, if the heart rate was 60–85 beats per minute (bpm), (2) prospective high-pitch spiral acquisition, if the heart rate was <60 bpm, (3) spiral acquisition with retrospective ECG gating, if the heart rate was >85 bpm. Contrast medium (Lopamiron370; Bracco, Milan, Italy) was injected with a speed of 3.5–5.5 ml/s and a volume of 50–80 ml for the contrast-enhanced scan. A slice thickness of 0.75 mm was used for image reconstruction. The reconstruction interval was 0.5 mm. A standard reconstruction algorithm (B26) was used at the best diastole or best systole phase.

Reconstruction of the CTA geometrical model

A validated software package (QAngio CT Research Edition version 2.1, Medis specials bv, Leiden, The Netherlands) was used to delineate the lumen of the interrogated vessel and its side branches from CTA images [19]. A well-trained and experienced radiologist specialist in cardiac imaging performed the analyses. This radiologist was blinded to the ICA images. A CTA geometrical model was created after lumen delineation with an in-house prototype software package (Q3DMerger). This software program automatically merged all luminal cross-sections of the vessel and its side branches into a tree structure [18].

ICA image acquisition and geometrical reconstruction

A monoplane or biplane X-ray system (AXIOM-Artis, Siemens; AlluraXper, Philips; DFP-8000D, TOSHIBA; Innova 3100, GE) was used to record the ICA images at 30 or 15 frames/s. The images were subsequently analyzed by an experienced analyst trained in 3D QCA. Two angiographic projects with minimal foreshortening and overlap were chosen and then 3D angiographic reconstruction was performed with a validated 3D QCA software package (QAngio XA 3D research edition 1.1, Medis special by Leiden, The Netherlands) [20, 21]. A 3D QCA geometrical model was generated by merging the reconstructed luminal cross-sections of the interrogated vessel with mild or intermediate de novo lesions and its side branches, using the Q3DMerger software. Stented vessels or vessels with prior coronary artery bypass surgery were not included for analysis.

Analysis of ESS

ANSYS ICEM 15.0 (ANSYS,Inc., Canonsburg, Pennsylvania) with tetrahedral cells (meshing) was used to discretize the 3D reconstructed geometries. For each model, volume tetrahedral meshes with approximately 200,000–2 million tetrahedral elements were created. In each cell, Navier Stokes equations were implemented and nonlinear partial differential equations were solved simultaneously with ANSYS FLUENT 15.0 (ANSYS, Inc). A viscosity of 0.0035 kg/m·s and blood density of 1060 kg/m^3 were used. The lumen wall was studied with a no-slip condition. The volumetric flow rate was estimated by means of the contrast transport time, calculated by frame counts and the 3D geometry reconstructed from two ICA images. Subsequently, it was applied as the inlet boundary condition of the CFD simulation [22]. The same inlet flow was used to calculate ESS_{CTA} and ESS_{ICA}. At the outflow boundaries, a fully developed flow condition was applied. As assessed by 3D angiography, vessel diameter and the bifurcation were used to determine the flow separation at the bifurcation [22]. In other words, we used the diameters of the daughter branches and the bifurcation angles to determine the flow separation [22]. Parallel computing and the finite volume method were used in the computation. Both the ESS_{CTA} and ESS_{ICA} corresponding to the CTA and 3D ICA geometrical model, respectively, were derived at each cell after the simulations. The lumen of the main vessel was divided into sections of 3-mm length and 30° arc-width to compare the ESS_{CTA} and ESS_{ICA} values [18]. For segment-per-segment comparisons, segments defined by the same consecutive side branches in the CTA and ICA models were matched and the corresponding mean, maximal and minimal ESS compared head-to-head between both models.

To investigate the impact of the inlet flow profile on the calculation of ESS, the steady flow was converted into pulsatile flow using a flow pattern derived from a previous study [23]. Specifically, the magnitude of the pulsatile flow was modulated in such a way that the average magnitude of the flow velocity over a cardiac cycle was equal to the steady flow velocity. Subsequently, the modulated pulsatile flow velocity was applied as the inlet boundary condition in the CFD computation. In this study, we randomly selected 10 coronary arteries and applied a pulsatile flow profile in the CFD simulation, from which ESS_{CTA} was derived and compared with the corresponding value derived from the steady flow CFD simulation.

Statistics

The continuous variables are shown as the mean ± SD or median (interquartile range [IQR]) as appropriate. Categorical variables are shown as counts (percentages). A

per-patient basis was used for data analysis for clinical characteristics. A per-segment basis was used for the comparison between ESS_{CTA} and ESS_{ICA}. Bland-Altman plots were used to determine the agreement between ESS_{CTA} and ESS_{ICA}. Pearson's correlation coefficients (r) were calculated to assess correlations. A t test or a non-parametric Wilcoxon-W test was used to compare paired variables, depending on the distribution. IBM SPSS software (version 20.0, SPSS Inc., Chicago, IL) was used for statistical analyses. A 2-sided p value of <0.05 was considered as significant.

Results

Baseline clinical and lesion characteristics

Tables 1 and 2 show the baseline characteristics of the included patients and the assessed vessels. Mild or intermediate lesions of 44 patients were included. Three patients were excluded as result of poor angiographic image quality and excessive overlap. Figure 1 shows the study flow chart. In the ESS_{CTA} and ESS_{ICA} comparisons, a total of 57 vessels (30 left anterior descending arteries, 3 left circumflex arteries, 24 right coronary arteries) from 41 patients were included. The mean systolic blood pressure of the patients was 137.2 ± 22.9 mmHg and the mean diastolic blood pressure was 73.0 ± 13.0 mmHg. The mean percent diameter stenosis (DS%) of the interrogated vessels was 43.4 ± 10.8 % and the minimum lumen area (MLA) was 2.38 ± 1.20 mm^2 (median 2.05 [IQR 1.50–3.03]). In the interrogated vessels, an average of 2.1 side branches (range, 0 to 5 side branches) was identified. By quantitative CTA, the median plaque volume (PV) was 272.9 mm^3 (IQR 192.0–411.8).

Table 1 Baseline clinical characteristics (n = 41)

Age (years)	68.0 ± 10.0
Male	30 (73.2 %)
Mean body mass index (kg/m^2)	25.4 (15.8–46.0)
Hypertension	35 (85.4 %)
Hyperlipidemia	18 (43.9 %)
Current smoker	8 (19.5 %)
Diabetes mellitus	12 (29.3 %)
Renal disease	9 (22.0 %)
Clinical syndrome type	
Stable symptoms	33 (80.5 %)
Unstable angina	7 (17.1 %)
Post myocardial infarction	1 (2.4 %)
Cardiovascular history	
Previous PCI	20 (48.8 %)
Pervious CABG	3 (7.3 %)

Values are mean ± SD, n(%), or median (IQR) *CABG* coronary artery bypass graft, *IQR* interquartile range, *PCI* percutaneous coronary intervention

Table 2 Baseline lesion characteristics (n = 56)

Index artery	
Left anterior descending artery	30 (52.6 %)
Left circumflex artery	3 (5.3 %)
Right coronary artery	24 (42.1 %)
Percent diameter stenosis	43.4 ± 10.8
Percent area stenosis	57.8 ± 15.0
Minimum lumen diameter (mm)	1.51 ± 0.38
Reference vessel diameter (mm)	2.70 ± 0.52
Minimum lumen area (mm^2)	2.05 (1.50–3.03)
Plaque volume (mm^3)	272.9 (192.0–411.8)
Lesion eccentricity index	0.27 ± 0.02

Values are n (%), or mean SD, median (IQR). Plaque volume was quantified by coronary computed tomography angiography. Other anatomical parameters were quantified by 3-dimensional quantitative coronary angiography. *IQR* interquartile range

Correlation and agreement between ESS_{CTA} and ESS_{ICA}

Figure 2 shows representative examples of computations of ESS_{CTA} and ESS_{ICA}. Fifty-seven vessels in 41 patients were analyzed. ESS_{CTA} and ESS_{ICA} were compared in 163 matched segments. Segment-based ESS_{CTA} and ESS_{ICA} results were similar (Table 3): mean ESS: 4.97 (4.37–5.57) Pascal versus 4.86 (4.27–5.44) Pascal, $p = 0.58$; minimal ESS: 0.86 (0.67–1.05) Pascal versus 0.79 (0.63–0.95) Pascal, $p = 0.37$; and maximal ESS: 14.50 (12.62–16.38) Pascal versus 13.76 (11.44–16.08) Pascal, $p = 0.44$. In addition, Table 4 shows that mean, minimal, and maximal values between ESS_{CTA} and ESS_{ICA} are also similar when stratified according to two different scanning methods: ADCT and DSCT. The correlation and agreement between the computed ESS_{CTA} and ESS_{ICA} results are presented in Fig. 3. Good correlations between the ESS_{CTA} and the ESS_{ICA} results were observed for the mean ($r = 0.75$, $p < 0.001$), minimal ($r = 0.61$, $p < 0.001$), and maximal ($r = 0.62$, $p < 0.001$) ESS values. Nevertheless, the Bland-Altman plot shows moderate agreement between the ESS_{CTA} and the ESS_{ICA}, with standard deviations of 2.70, 1.03 and 12.09, respectively.

Comparison between pulsatile and steady flow simulations

There was no substantial deviation between ESS computations based on pulsatile and steady inlet flows in terms of their mean and minimum ESS values; however, the

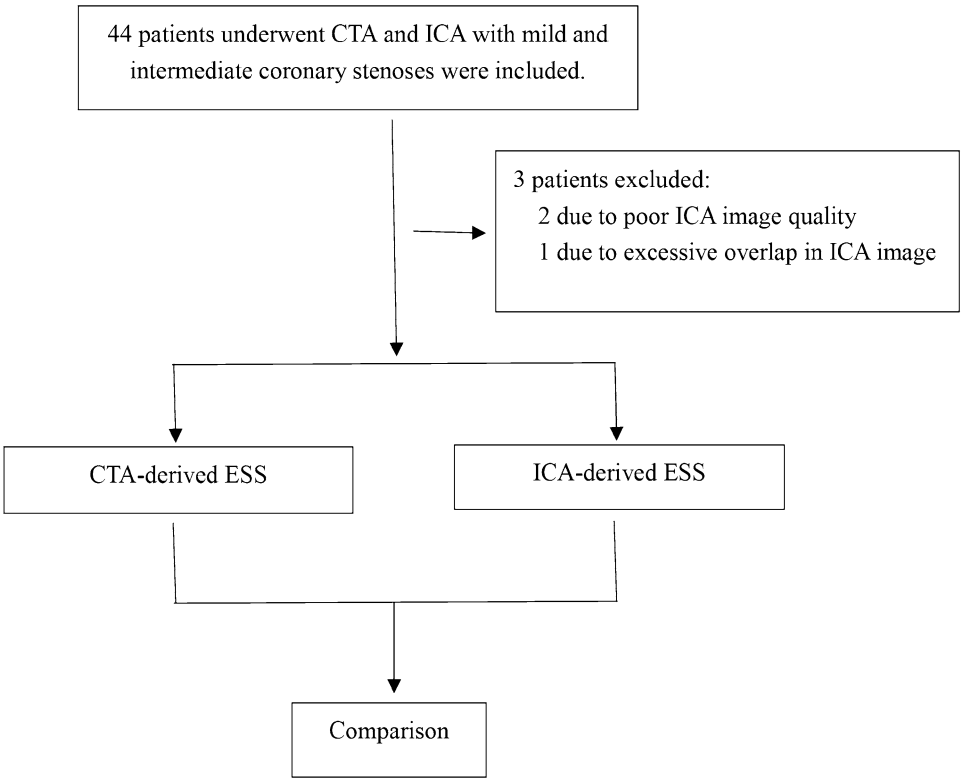

Fig. 1 Study flow chart. *CTA* computed tomography angiography, *ICA* invasive coronary angiography, *ESS* endothelial shear stress

deviation in the maximum ESS values show wider scatter, despite being statistically nonsignificant (Table 5). Table 6 shows the comparison in each case. Of note, the maximum ESS value increased substantially in individual cases when applying the pulsatile inlet flow.

The mean computational time was approximately 10 min and 3 h for CFD analysis using steady inlet flow and pulsatile inlet flow, respectively, on a workstation with a quad-core Intel Core™2 Duo Processor I7-6700 (Intel Corporation, Santa Clara, California; 3.4 GHz) and 16 GB of RAM.

Discussion

In the present study, we developed a CTA-based computational method for in vivo assessment of ESS and compared the CTA-derived ESS (ESS_{CTA}) with ICA-derived ESS (ESS_{ICA}). The main findings can be summarized as follows: (1) In a study population with mild and intermediate coronary stenosis, segment-based ESS_{CTA} and ESS_{ICA} were similar, in terms of their mean, minimal, and maximal values, (2) ESS_{CTA} and ESS_{ICA} had reasonably good correlations for the mean ($r=0.75$, $p<0.001$), minimal ($r=0.61$, $p<0.001$), and maximal ($r=0.62$, $p<0.001$) ESS values, (3) The mean ESS values were not substantially different, while the maximum ESS values deviated substantially in individual cases between the two CFD approaches that applied pulsatile and steady inlet flows.

Early identification of abnormal ESS patterns and rapid changes in plaque morphology might enable identification of the early stages of plaques that will evolve into a high-risk, rupture-prone lesion. A detailed assessment of blood flow pattern in coronary arteries requires accurate 3D reconstruction of the arterial lumen. Most CFD analyses have relied on invasive imaging techniques, such as OCT, IVUS and 3D QCA [3, 13, 24] that were applicable to high-risk patient populations. On the other hand, identification of an abnormal ESS would be particularly interesting in low-to-intermediate risk patients who might require special management when an abnormal ESS is identified. Coronary CTA has been increasingly used in scanning patients with suspected coronary artery disease (CAD) and several CTA-based ESS computational approaches have been reported [14–16, 25]. Coronary CTA also facilitates non-invasive assessment of plaque characteristics. In patients with suspected CAD, CTA-derived features of high-risk plaque consisting of positive vessel remodelling (PR) or low attenuation plaque (LAP) with <30HU appeared to be an incremental risk in predicting the onset of acute coronary syndrome [26]. This was partially supported by the fact that both PR and LAP were associated with inducible myocardial ischemia by invasive fractional flow reserve as a gold standard [27]. Given the nature of our analysis only using extracted

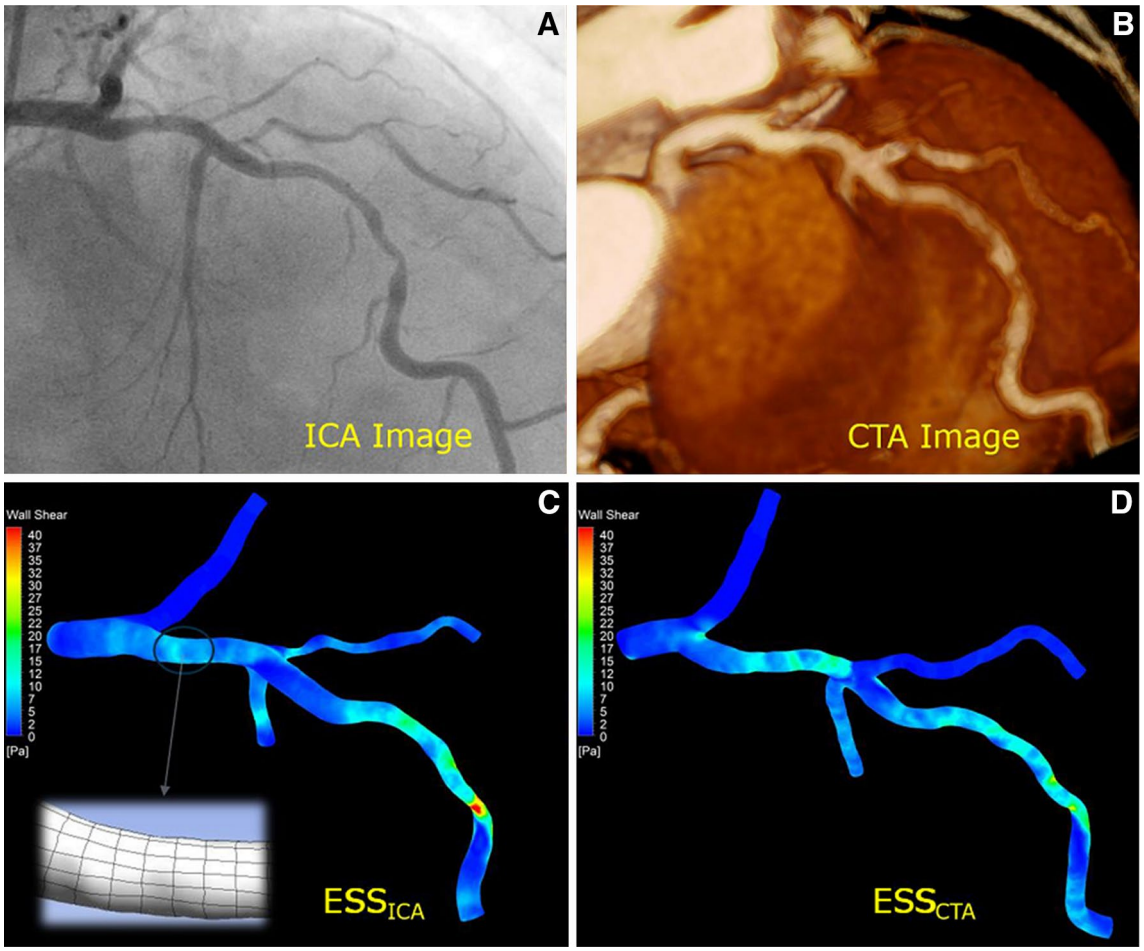

Fig. 2 Computations of ESS from ICA and CTA images. **a** ICA image shows the presence of an intermediate LAD lesion. **b** 3D rendering of the CTA image from the same patient. **c** ESS_{ICA} distribution superimposed on the coronary tree extracted from the ICA image. *Left bottom* shows the small portions in the grid where ESS was calculated. **d** ESS_{CTA} distribution superimposed on the coronary tree extracted from the CTA image. ESS_{ICA} ESS derived from ICA, ESS_{CTA} ESS derived from CTA, *CTA* computed tomography angiography, *ICA* invasive coronary angiography, *ESS* endothelial shear stress

lumen geometry, it might help better prediction of atherosclerotic plaque evolution or future coronary events to combine plaque characteristics assessment with focal ESS analysis that can be fully addressed in a non-invasive approach with CTA. However, to the best of our knowledge, there is no direct comparison of ESS computations applied to coronary tree models that are extracted from both CTA and ICA. In the current study, we used a validated computational approach [13, 22] to derive ESS from ICA images and compared it with ESS_{CTA}. Our results showed that segment-based ESS values were not significantly different when computed from CTA and ICA images. Nevertheless, the segment-based comparison might not represent the detailed comparison between small regions/portions with customized longitudinal length and arc-width. Due to the challenge in the co-registration of the individual small portions from CTA and ICA, we were not able to compare ESS_{CTA} and ESS_{ICA} in the portion level. Therefore, our results should be interpreted with caution.

So far, computation of coronary ESS has often relied on invasive procedures such as QCA, IVUS and OCT, which are adequate in a high risk patient population [1–6, 19, 28]. Patients with suspected CAD often undergo coronary CTA as part of the work-up for further diagnosis and many patients of low-to-intermediate risk are identified. Thus, ESS analysis based on non-invasive coronary CTA images can be a valuable tool for management of such patient populations. To date, the methodologies to characterize local ESS distributions have been used for research purposes only, because no tools were available to support online ESS computation. Attempts are underway to speed up the patient-specific 3D reconstruction and the CFD simulation. Using steady inlet flow instead of pulsatile inlet flow could greatly speed up the simulation. However, it remains unknown whether the ESS values will be

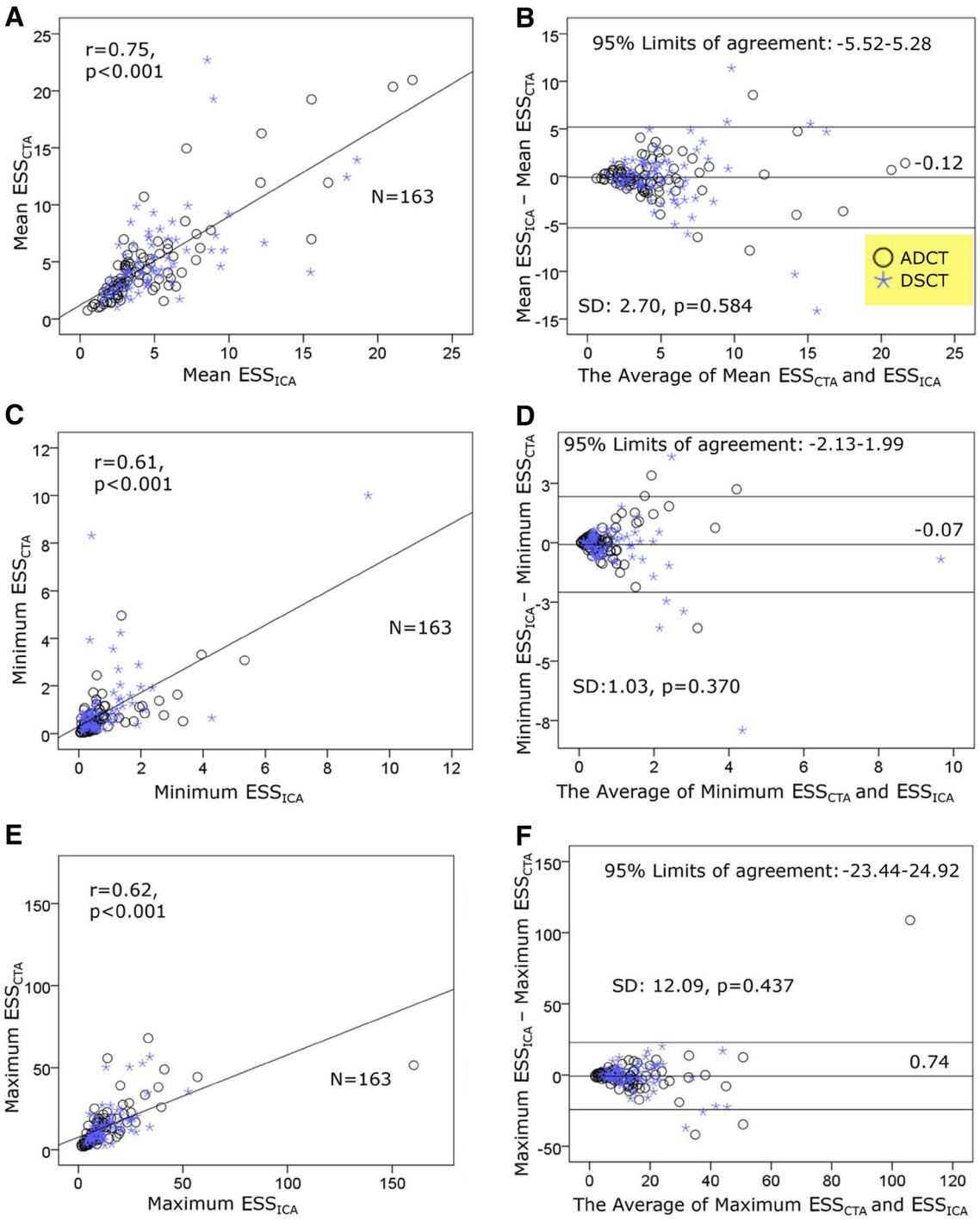

Fig. 3 Correlation and agreement between ESS_{CTA} and ESS_{ICA} in terms of mean, minimum and maximum values. Good correlations (r = 0.75, 0.61 and 0.62, respectively) were observed (**a, c, e**). Nevertheless, the Bland-Altman plot showed moderate agreements, with standard deviations of 2.70, 1.03 and 12.09, respectively (**b, d, f**). ESS_{ICA} ESS derived from ICA, ESS_{CTA} ESS derived from CTA, *CTA* computed tomography angiography, *ICA* invasive coronary angiography, *ESS* endothelial shear stress

affected in the relevant patient population. In this study, we found that there was no significant difference between ESS computations based on pulsatile and steady inlet flows, in terms of their mean and minimum ESS values; however, the deviation in the maximum ESS values show wider scatter. The maximum ESS differed substantially in individual patients when applying the two different inlet flow profiles. The possible reason for this phenomenon might

Table 3 Comparison between ESS_{CTA} and ESS_{ICA} (n = 163)

	ESS_{CTA} (Pa)	ESS_{ICA} (Pa)	*P*
Mean	4.97 (4.37–5.57)	4.86 (4.27–5.44)	0.58
Minimum	0.86 (0.67–1.05)	0.79 (0.63–0.95)	0.37
Maximum	14.50 (12.62–16.38)	13.76 (11.44–16.08)	0.44

Mean, minimal, and maximal values between ESS_{CTA} and ESS_{ICA} are similar

Table 4 Comparison between ESSCTA and ESSICA stratified according to type of CT scanner

	ESSCTA (Pa)	ESSICA (Pa)	*P*
ADCT (n = 89)			
Mean	4.71 (3.85–5.57)	4.61 (3.76–5.47)	0.67
Miniimum	0.66 (0.51–0.82)	0.73 (0.54–0.92)	0.43
Maximum	14.15 (11.46–16.84)	13.46 (9.55–17.38)	0.65
DSCT (n = 74)			
Mean	5.29 (4.44–6.14)	5.15 (4.36–5.94)	0.72
Minimum	1.10 (0.73–1.48)	0.87 (0.59–1.15)	0.11
Maximum	14.92 (12.27–17.56)	14.12 (11.99,16.24)	0.46

Mean, minimal, and maximal values between ESS_{CTA} and ESS_{ICA} are also similar when stratified according to two different scanning methods: ADCT and DSCT

Table 5 Comparison between the steady ESS and pulsatile ESS derived from CTA (n = 10)

	Steady	Pulsatile	*P*
ESS_{Mean} (Pa)	4.21 ± 2.04	3.97 ± 2.05	0.40
ESS_{Min} (Pa)	0.02 ± 0.02	0.02 ± 0.06	0.95
ESS_{Max} (Pa)	80.91 ± 52.70	145.76 ± 156.13	0.12

Mean, minimal, and maximal values between steady and pulsatile are similar

be as follows: coronary flow varies substantially during the whole cardiac cycle. It is reflected in the pulsatile flow profile but not in the steady flow. Therefore, the maximum flow velocity of pulsatile flow will be much higher than the mean flow velocity. Since ESS is closely related to the flow velocity [13], the maximum ESS will likely be higher when applying pulsatile inlet flow. In addition, higher flow velocity likely increases flow disturbance in the stenotic segment, resulting in higher ESS at specific spots while reducing ESS at other spots.

Limitations

The present study is not without limitations. It was a retrospective study with a small sample size and underrepresentation of the left circumflex coronary artery. Patients with mild or intermediate stenoses were not consecutively included. Thus, selection bias cannot be excluded. We did not include correction for clustering in the statistical analysis of ESS. However, we expect that the correction for clustering will have little impact on the result, since the number of segments per vessel is limited as we only analyzed the stenotic segments with large side branches. We compared the CTA-derived ESS with ICA-derived ESS, an imaging modality with lower image resolution compared with OCT. And the assumption of elliptical cross-sections in 3D angiographic reconstruction has limited the accuracy of ICA-derived ESS. Nevertheless, OCT imaging was often performed in high-risk patient populations and the ICA-derived ESS that applied in this study was recently shown to have good agreement with OCT-derived ESS [24, 28]. In addition, we only assessed vessels with de novo lesions without prior PCI and the impact of the presence of heavy calcification on the results of this study was not studied. Finally, we did not use a patient-specific flow profile measured by invasive Doppler wires but a fixed pulsatile pattern

Table 6 Calculation of ESS_{CTA} based on steady and pulsatile inlet flows

Case	ESS_{Mean} (Pa)		ESS_{Min} (Pa)		ESS_{Max} (Pa)	
	Steady	Pulsatile	Steady	Pulsatile	Steady	Pulsatile
1	4.45	3.01	0.01	0.00	38.81	68.28
2	4.14	4.25	0.01	0.01	52.04	86.24
3	1.85	1.95	0.03	0.00	158.88	138.60
4	3.17	3.59	0.02	0.00	43.66	73.58
5	4.75	3.17	0.02	0.01	57.99	89.00
6	1.99	2.53	0.01	0.01	89.70	70.51
7	6.90	5.86	0.03	0.00	159.72	541.02
8	6.21	5.75	0.01	0.01	140.75	287.90
9	7.00	8.08	0.01	0.00	27.13	24.72
10	1.68	1.49	0.08	0.19	40.44	77.77

with the average magnitude modulated to the average flow velocity per vessel. Therefore, possible errors in computation of ESS by the pulsatile flow cannot be completely excluded.

Conclusions

In vivo assessment of ESS from coronary CTA data is feasible. Our results suggest that geometrical reconstruction by CTA yields similar results to ICA in terms of segment-based ESS calculation in patients with mild or intermediate coronary stenoses. Thus, it has the potential to allow combined local hemodynamic and plaque morphologic information for risk stratification in patients suggestive of coronary artery disease.

Acknowledgments The authors acknowledged Saeb R. Lamooki for his contribution in preparing the manuscript and data management. S. Tu acknowledges the support by The Program for Professor of Special Appointment (Eastern Scholar) at Shanghai Institutions of Higher Learning, The Shanghai Pujiang Program (No. 15PJ1404200), the National Natural Science Foundation of China (Grants 31500797 and 81570456) and the National Key Research Program of China (Grant 2016YFC0100500). W. Yang acknowledges the support by the National Natural Science Foundation of China (Grants 81501467). J. Pu acknowledges the support by the National Science Fund for Distinguished Young Scholars (81625002), Program for New Century Excellent Talents in University from Ministry of Education of China (NCET-12-0352), Shanghai Shuguang Program (12SG22) and Shanghai Gaofeng Clinical Medicine Program (20152209).

Compliance with ethical standards

Conflict of interest Y. Li and P. Kitslaar are employed by Medis medical imaging systems bv and have a research appointment at the Leiden University Medical Center (LUMC). John H. C. Reiber is the CEO of Medis, and has a part-time appointment at LUMC as Prof of Medical Imaging. S. Tu receives research grant support from Medis. All other authors declare that they have no conflict of interest.

References

1. Malek AM et al (1999) Hemodynamic shear stress and its role in atherosclerosis. JAMA 282(1):2035–2042
2. Cheng C et al (2006) Atherosclerotic lesion size and vulnerability are determined by patterns of fluid shear stress. Circulation 113(23):2744–2753
3. Samady H et al (2011) Coronary artery wall shear stress is associated with progression and transformation of atherosclerotic plaque and arterial remodeling in patients with coronary artery disease. Circulation 124(7):779–788
4. Chatzizisis YS et al (2008) Prediction of the localization of high-risk coronary atherosclerotic plaques on the basis of low endothelial shear stress: an intravascular ultrasound and histopathology natural history study. Circulation 117(8):993–1002
5. Frangos SG, Gahtan V, Sumpio B (1999) Localization of atherosclerosis: role of hemodynamics. Arch Surg 134(10):1142–1149
6. Chatzizisis YS et al (2007) Role of endothelial shear stress in the natural history of coronary atherosclerosis and vascular remodeling: molecular, cellular, and vascular behavior. J Am Coll Cardiol 49(25):2379–2393
7. Wentzel JJ et al (2003) Extension of increased atherosclerotic wall thickness into high shear stress regions is associated with loss of compensatory remodeling. Circulation 108(1):17–23
8. Asakura T, Karino T (1990) Flow patterns and spatial distribution of atherosclerotic lesions in human coronary arteries. Circ Res 66(4):1045–1066
9. Tadjfar M (2004) Branch angle and flow into a symmetric bifurcation. J Biomech Eng 126(4):516–518
10. Krams R (1997) Evaluation of endothelial shear stress and 3D geometry as factors determining the development of atherosclerosis and remodeling in human coronary arteries in vivo. Combining 3D reconstruction from angiography and IVUS (ANGUS) with computational fluid dynamics. Arterioscler Thromb Vasc Biol 17(10):2061–2065
11. Stone PH et al (2012) Prediction of progression of coronary artery disease and clinical outcomes using vascular profiling of endothelial shear stress and arterial plaque characteristics: the PREDICTION Study. Circulation 126(2):172–181
12. Stone PH et al (2007) Regions of low endothelial shear stress are the sites where coronary plaque progresses and vascular remodelling occurs in humans: an in vivo serial study. Eur Heart J 28(6):705–710
13. Li Y et al (2015) Impact of side branch modeling on computation of endothelial shear stress in coronary artery disease: coronary tree reconstruction by fusion of 3D angiography and OCT. J Am Coll Cardiol 66(2):125–135
14. Frauenfelder T et al (2007) In-vivo flow simulation in coronary arteries based on computed tomography datasets: feasibility and initial results. Eur Radiol 17(5):1291–1300
15. Frauenfelder T et al (2007) Flow and wall shear stress in end-to-side and side-to-side anastomosis of venous coronary artery bypass grafts. Biomed Eng Online 6:35
16. Goubergrits L et al (2008) CFD analysis in an anatomically realistic coronary artery model based on non-invasive 3D imaging: comparison of magnetic resonance imaging with computed tomography. Int J Cardiovasc Imaging 24(4):411–421
17. Giannopoulos AA et al (2016) Quantifying the effect of side branches in endothelial shear stress estimates. Atherosclerosis 251:213–218
18. Liu L et al (2016) The impact of image resolution on computation of fractional flow reserve: coronary computed tomography angiography versus 3-dimensional quantitative coronary angiography. Int J Cardiovasc Imaging 32(3):513–523
19. De Graaf MA et al (2013) Automatic quantification and characterization of coronary atherosclerosis with computed tomography coronary angiography: cross-correlation with intravascular ultrasound virtual histology. Int J Cardiovasc Imaging 29(5):1177–1190
20. Tu S et al (2012) In vivo comparison of arterial lumen dimensions assessed by co-registered three-dimensional (3D) quantitative coronary angiography, intravascular ultrasound and optical coherence tomography. Int J Cardiovasc Imaging 28(6):1315–1327
21. Tu S et al (2016) Diagnostic accuracy of fast computational approaches to derive fractional flow reserve from diagnostic coronary angiography: the international multicenter FAVOR pilot study. JACC Cardiovasc Interv 9(19):2024–2035
22. Tu S et al (2014) Fractional flow reserve calculation from 3-dimensional quantitative coronary angiography and TIMI frame count: a fast computer model to quantify the functional significance of moderately obstructed coronary arteries. JACC Cardiovasc Interv 7(7):768–777

23. Barlis P et al (2015) Reversal of flow between serial bifurcation lesions: insights from computational fluid dynamic analysis in a population-based phantom model. EuroIntervention 11(5):e1–e3
24. Toutouzas K et al (2015) Accurate and reproducible reconstruction of coronary arteries and endothelial shear stress calculation using 3D OCT: comparative study to 3D IVUS and 3D QCA. Atherosclerosis 240(2):510–519
25. Hetterich H et al (2015) Coronary computed tomography angiography based assessment of endothelial shear sress and its association with atherosclerotic plaque distribution in-vivo. PLoS One 10(1):e0115408
26. Motoyama S et al (2009) Computed tomographic angiography characteristics of atherosclerotic plaques subsequently resulting in acute coronary syndrome. J Am Coll Cardiol 54(1):49–57
27. Park HB et al (2015) Atherosclerotic plaque characteristics by CT angiography identify coronary lesions that cause ischemia: a direct comparison to fractional flow reserve. JACC Cardiovasc Imaging 8(1):1–10
28. Chatzizisis YS et al (2016) Association of global and local low endothelial shear stress with high-risk plaque using intracoronary 3D optical coherence tomography: Introduction of 'shear stress score'. Eur Heart J Cardiovasc Imaging. doi:10.1093/ehjci/jew134